 

*NONLINEAR OPTICAL PHENOMENA*

PACS numbers: 42.50.Hz; 42.50.Md; 42.25.Ja
DOI: 10.1070/QE2009v039n09ABEH013935

# Numerical simulation of nonstationary effects of radiation polarisation for the Λ interaction scheme in the case of degenerate energy levels

A.V. Volkov, N.A. Druzhinina, O.M. Parshkov

*Abstract*. **Nonstationary polarisation effects in a medium with the Λ-scheme of energy levels with the quantum numbers of the total angular momentum equal to 0, 2, and 1 are numerically simulated. The analysis is performed in the slowly varying envelope approximation taking into account the inhomogeneous broadening of quantum transition lines. It is assumed that the lower-frequency (signal) radiation at the input to a resonance medium is considerably weaker than the higher-frequency (pump) radiation. It is shown that the polarisation of the signal pulse inside the medium is quasi-elliptic in the general case and is independent of the input-pulse polarisation. If the 'area' of the input pump pulse in the absence of signal radiation admits the formation of only one 2π-pulse, then the major axes of polarisation ellipses for the signal inside the medium and input pump radiation are collinear, however, the directions of rotation of the electric field strengths of these radiations are mutually opposite. For higher-power pump pulses, the polarisation structure of the signal pulse in the medium becomes considerably more complicated.**

***Keywords***: *degeneracy of energy levels, nonstationary radiation polarisation, inhomogeneous broadening*.

## 1. Introduction

Systems of two or three nondegenerate energy levels are simplest and therefore are most often used as models of quantum objects in the theory of nonstationary resonance interaction of laser radiation with matter. Within the framework of these models, the main results have been obtained in the studies of photon echo [1], self-induced transparency (SIT) [2], and electromagnetically induced transparency (EIT) [3].

However, in most cases the energy spectrum of quantum objects consists of degenerate energy levels. A special choice of the polarisation states (linear or circular) of laser radiation allows one often, but not always, to study its resonance interaction with a medium within the framework of models with nondegenerate energy levels. In this case, polarisation effects, i.e. effects related to a change in the polarisation of radiation during its propagation are not considered.

This circumstance stimulated the development of the theory of nonstationary resonance interaction of pulsed laser radiation with quantum transitions between degenerate energy levels. The influence of the degeneracy of levels on SIT in the radiation field with linear or circular polarisation was investigated in [4 – 6]. In a number of papers (see review [7]), polarisation effects related to SIT at the quantum transition between degenerate energy levels were considered. Electromagnetically induced transparency in this scheme was studied in [8 – 10]. The coherent two-field spectroscopy of a quantum transition between degenerate energy levels was investigated in [11]. In [12, 13], the integrability of the system of equations of the double resonance at degenerate energy levels by the method of inverse scattering problem was proved and the simulton solutions of these equations were studied.

In this paper, we studied theoretically polarisation effects appearing in the nonstationary interaction of two laser radiations with an ensemble of tree-level quantum objects in the presence of degeneracy in the case of the Λ-configuration of interaction. Unlike studies [12, 13], we took into account the inhomogeneous broadening of quantum transition lines and did not assume that the oscillator strengths of these transitions were identical. We assume that the levels are characterised by the total angular momenta $J = 0$, 2, and 1 with increasing their energy, and the upper level is shared by two resonantly excited quantum transitions.

By assuming that the change in the state of each quantum object occurs quite rapidly, we neglect relaxation processes. By considering a rarefied gas as a resonance medium, we take into account the Doppler broadening of spectral lines. The signal radiation incident on the medium is assumed so weak that it should not affect in fact the evolution of the pump radiation at the initial interaction stage. Simulations were performed for the Λ-scheme of levels of the $^{208}$Pb isotope, in which the EIT of circularly polarised laser fields was observed [14].

The theoretical study of nonstationary resonance interactions of two laser fields with fixed polarisation states (circular or collinear linear) with an ensemble of quantum objects with three nondegenerate quantum levels resulted in the description of the effects opening up the new possibilities for recording and reading information on light pulses [15 – 17], creating the quantum memory [18], controlling laser radiation parameters [19, 20], and probing ultracold atoms and molecular clouds [21]. These effects are based on

**A.V. Volkov, N.A. Druzhinina, O.M. Parshkov** Saratov State Technical University, ul. Politekhnicheskaya 77, 410054 Saratov, Russia; e-mail: wolkowaw@yandex.ru

Received 27 June 2008; revision received 26 January 2009
*Kvantovaya Elektronika* **39** (9) 845 – 852 (2009)
Translated by M.N. Sapozhnikov

the possibility of controlling the intensity of one frequency component of the field by varying the intensity of another component.

The study presented here was motivated, aside from the cognitive aspect, by the following. The elliptically polarised frequency components of radiation considered in our paper are characterised, along with their intensity, by the parameters of their polarisation ellipses. There exists the possibility to control not only the radiation intensity but also these parameters for one frequency component by varying the parameters of the polarisation ellipse of another frequency component. This possibility was confirmed experimentally for the quasi-static EIT regime [22]. This circumstance suggests that the scope of practical applications of the nonstationary resonance interaction of the two-frequency laser field with an ensemble of three-level quantum objects can be extended.

## 2. Formulation of the boundary problem

Figure 1 presents the Λ-scheme consisting of the non-degenerate lower level ($J = 0$), five-fold degenerate middle level ($J = 2$), and triply degenerate upper level ($J = 1$). Such a Λ-scheme is formed, for example, by the $6p^2\ ^3P_0$, $6p^2\ ^3P_2$, $6p7s\ ^3P_1^o$ levels of the $^{208}Pb$ isotope. Let us take the $z$ axis as the quantisation axis and denote by $M$ the quantum number of projections of the total angular momentum on this axis. The possible values of $M$ for each of the tree levels of the Λ-scheme are indicated in Fig. 1. Let $\phi_k$ ($k = 1, 2, ..., 9$) be the orthonormalised set of the common eigenfunctions of the Hamiltonian, and the operators of the total angular momentum and its projection on the $z$ axis for an isolated atom. The function $\phi_1$ corresponds to the $J = 0$ level, functions $\phi_k$ ($k = 2, 3, 4$) correspond to the $J = 1$ level, and functions $\phi_k$ ($k = 5, 6, ..., 9$) – to the $J = 2$ level (see Fig. 1). Let $D_1$ and $D_2$ be the reduced electric dipole moments for transitions $J = 0 \to J = 1$ and $J = 2 \to J = 1$, respectively, and $\omega_1$ and $\omega_2$ are the frequencies of these transitions for an atom at rest. Assuming that the resonance medium is a rarefied gas, we introduce the parameter $T_1 = 2/\Delta_1$, where $\Delta_1$ is the width (at the $e^{-1}$ level) of the Doppler density distribution of the $J = 0 \to J = 1$ transition frequencies $\omega_1'$.

Consider an ensemble of Λ-schemes irradiated by two arbitrarily polarised plane quasi-monochromatic coherent laser waves with frequencies $\omega_1$ and $\omega_2$ propagating along the $z$ axis, so that the total electric field can be written in the form

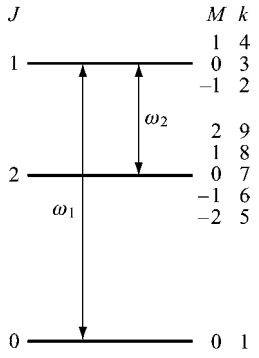


**Figure 1.** Λ-configuration of quantum transitions between energy levels with $J = 0$, $J = 2$, and $J = 1$; $k$ is the number of the state in the mathematical model.

$$\boldsymbol{E} = \sum_{l=1}^{2} \mu_l [\boldsymbol{i} E_{xl} \cos(\omega_l t - k_l z + \delta_{xl}) + \boldsymbol{j} E_{yl} \cos(\omega_l t - k_l z + \delta_{yl})]. \quad (1)$$

Here, $\mu_l = \hbar\sqrt{2l+1}/(|D_l|T_1)$ are the normalisation constants; $\boldsymbol{i}$ and $\boldsymbol{j}$ are the unit vectors of the $x$ and $y$ axes; $E_{xl}$, $E_{yl}$, $\delta_{xl}$, $\delta_{yl}$ are functions depending on $z$ and $t$, which describe the amplitudes and phases of oscillations of the $x$ and $y$ field components; and $k_l = \omega_l/c$. Below, we will call the field with frequency $\omega_1$ the pump, and the field with frequency $\omega_2$ – the signal.

The wave function can be written in the form

$$\Psi = \bar{c}_1\phi_1 + \left(\sum_{k=2}^{4} \bar{c}_k\phi_k\right)\exp(-i\xi_1) + \left(\sum_{k=5}^{9} \bar{c}_k\phi_k\right)\exp\left[-i(\xi_1 - \xi_2)\right], \quad (2)$$

where $\xi_l = \omega_l t - k_l z$; $l = 1,2$. Note that we consider the probability amplitudes $\bar{c}_k$ as functions of variables $z$ and $t$. Let us introduce the complex field variables $f_l$ and $g_l$ ($l = 1, 2$) by the expressions

$$f_l = \left[E_{xl}\exp(i\delta_{xl}) - iE_{yl}\exp(i\delta_{yl})\right]/\sqrt{2},$$

$$g_l = \left[E_{xl}\exp(-i\delta_{xl}) - iE_{yl}\exp(-i\delta_{yl})\right]/\sqrt{2},$$

and the modified probability amplitudes

$$c_1 = -2\bar{c}_1 \arg D_1,\ c_2 = \bar{c}_2,\ c_4 = \bar{c}_4,\ c_5 = 2\bar{c}_5 \arg D_2,,$$

$$c_7 = (2/\sqrt{6})\bar{c}_7 \arg D_2,\ c_9 = 2\bar{c}_9 \arg D_2,$$

where $\arg a$ is the argument of a complex number $a$. Let us introduce the normalised independent variables $s$ and $w$

$$s = z/z_0,\ w = (t - z/c)/T_1, \quad (3)$$

where $z_0 = 3\hbar c/(2\pi N|D_1|^2 T_1\omega_1)$ and $N$ is the concentration of atoms. By describing the evolution of the filed and quantum objects by the Maxwell and Schrödinger equations, respectively, we obtain, in the slowly varying amplitude approximation, the system of equations

$$\frac{\partial f_1}{\partial s} = \frac{i}{\sqrt{\pi}}\int_{-\infty}^{+\infty} c_1 c_2^* \exp(-\varepsilon_1^2)d\varepsilon_1,$$

$$\frac{\partial f_2}{\partial s} = -\frac{i}{\sqrt{\pi}}\xi\int_{-\infty}^{+\infty} (c_4^* c_9 + c_2^* c_7)\exp(-\varepsilon_1^2)d\varepsilon_1,$$

$$\frac{\partial g_1}{\partial s} = \frac{i}{\sqrt{\pi}}\int_{-\infty}^{+\infty} c_1^* c_4 \exp(-\varepsilon_1^2)d\varepsilon_1,$$

$$\frac{\partial g_2}{\partial s} = -\frac{i}{\sqrt{\pi}}\xi\int_{-\infty}^{+\infty} (c_2 c_5^* + c_4 c_7^*)\exp(-\varepsilon_1^2)d\varepsilon_1,$$

$$\frac{\partial c_1}{\partial w} = -i(f_1 c_2 - g_1^* c_4), \quad (4)$$

$$\frac{\partial c_2}{\partial w} + i\varepsilon_1 c_2 = -\frac{i}{4}(f_1^* c_1 + g_2 c_5 - f_2^* c_7),$$

$$\frac{\partial c_4}{\partial w} + i\varepsilon_1 c_4 = \frac{i}{4}(g_1 c_1 - g_2 c_7 + f_2^* c_9),$$

$$\frac{\partial c_5}{\partial w} + i\varepsilon_1(1-\beta)c_5 = -ig_2^* c_2,$$

$$\frac{\partial c_7}{\partial w} + i\varepsilon_1(1-\beta)c_7 = \frac{i}{6}(f_2 c_2 - g_2^* c_4),$$

$$\frac{\partial c_9}{\partial w} + i\varepsilon_1(1-\beta)c_9 = if_2 c_4,$$

$$\beta = \frac{\omega_2}{\omega_1},\ \xi = \frac{3}{5}\frac{\omega_2|D_2|^2}{\omega_1|D_1|^2}. \quad (5)$$

For the chosen transitions in the $^{209}$Pb isotope, we have $\beta = 0.7$ and $\xi = 2.11$. These estimates were obtained by using data from [23].

Note that the amplitudes $\bar{c}_3$, $\bar{c}_6$, and $\bar{c}_8$ do not enter in system (4). Their evolution is determined by a closed system of three differential equations, which for the initial conditions $\bar{c}_3 = \bar{c}_6 = \bar{c}_8 = 0$ accepted below, has the solution $\bar{c}_3 = \bar{c}_6 = \bar{c}_8 = 0$ for all $s$ and $w$. The integrals in the right-hand sides of the first four equations of system (4), which follow from Maxwell equations, appear due to the consideration of the Doppler inhomogeneous broadening of transition lines. In this case, $\varepsilon_1 = T_1(\omega_1' - \omega_1)$.

We will analyse the solutions of system (4) in terms of the parameters $a_l$, $\alpha_l$, $\gamma_l$ of the polarisation ellipse (PE) of pump radiation ($l = 1$) and signal radiation ($l = 2$). Here, $a_l$ is the major semiaxis of the PE measured in units of $\mu_l$; $\alpha_l$ is its inclination angle with respect to the $x$ axis; and $\gamma_l$ is the ellipse compression parameter. According to usual standards [24], we have $a_l \geqslant 0$, $0 \leqslant \alpha_l < \pi$, $-1 \leqslant \gamma_l \leqslant 1$. The parameter $|\gamma_l|$ is the ratio of the minor axis of the PE to its major axis. The condition $0 < \gamma_l < 1$ ($-1 < \gamma_l < 0$) corresponds to the right-hand (left-hand) elliptic polarisation, while the condition $\gamma_l = 0$ corresponds to linearly polarised radiation. For $|\gamma_l| = 1$ (circular polarisation), the angle $\alpha_l$ is not defined, and we assign formally to it the negative value $\alpha_l = -0.2$.

By specifying the PE parameters ($a_l$, $\alpha_l$, $\gamma_l$ and one of the phases, for example, $\delta_{xl}$), we can determine uniquely the values of $f_l$ and $g_l$. The corresponding expressions are too cumbersome and are omitted here. The PE parameters are generally the functions of $s$ and $w$. We will call polarisation states with slowly varying parameters $\alpha_l$ and $\gamma_l$ the quasi-elliptic states, similarly to a harmonic oscillation with the slowly varying amplitude, which is called the quasi-harmonic oscillation. Below, the function $a_l(s, w)$ for $l = 1$ is called the pump envelope and for $l = 2$ – the signal envelope.

The initial conditions ($w = 0$) for system (4) are specified in the form

$$c_1/2 = 1,\ c_2 = c_4 = c_5 = c_7 = c_9 = 0,\ s \geqslant 0,$$

which corresponds to the state in which all the atoms occupy the lower energy level at the initial instant of time. The boundary conditions ($s = 0$) are specified by the expressions

$$\alpha_l = \alpha_{l0},\ \gamma_l = \gamma_{l0},\ \delta_{xl} = 0, \quad (6)$$

$$a_1 = a_{10}\,\mathrm{sech}(w - 7),\ a_2 = 10^{-10},\ w \geqslant 0, \quad (7)$$

where $l = 1, 2$; and $\alpha_{l0}$ and $\gamma_{l0}$ are constants. Equalities (6) correspond to input laser pulses with the constant orientation of the major axis and constant eccentricity of the PE. Equalities (7) simulate the situation when the bell-shaped input pump pulse has the duration equal approximately to $2T_1$, whereas the input signal pulse has a considerably longer duration and so weak that its presence near the input to the medium does not affect the evolution of the pump pulse.

As the integral parameters of the pulses, we will use parameters $W_l$ and $I_l$ ($l = 1, 2$), which are proportional to the energy and the $z$ component of the angular momentum of pump ($l = 1$) and signal ($l = 2$) radiation per unit cross section.

The problem of the degenerate $J = 0 \leftrightarrow J = 1$ transition (in our case, this is the pump transition, for which $l = 1$) admits, according to the SIT theory, the solution in the form of the $2\pi$-pulse [10]. Let us denote the parameters of the $2\pi$-pulse by the subscript 1 and note that $\alpha_1$ and $\gamma_1$ are constant for this pulse, while $\gamma_1$, $a_{1m}$ (the maximum value of the envelope), $\tau_1$ (duration at the sech1 level), and $v_1$ (velocity in coordinates $s$ and $w$) are related by the expression

$$\tau_1 = 2/r,\ v_1 = \sqrt{\pi}\left[\frac{4}{r^2}\int_{-\infty}^{+\infty}\frac{\exp(-\varepsilon_1^2)\,d\varepsilon_1}{1 + 4\varepsilon_1^2/r^2}\right]^{-1}, \quad (8)$$

where $r = a_{1m}\sqrt{1 + \gamma_1^2}$.

Let us assume that the numerical simulation gives a pulse at the pump frequency with constants $\alpha_1$ and $\gamma_1$, the envelope with the invariable symmetric bell-shaped contour and the constant maximum value $a_{1m}$. We assume that this pulse is the $2\pi$-pulse if $\tau_1$ and $v_1$ calculated by these values of $a_{1m}$ and $\gamma_1$ from (8) differ from their values obtained in simulations no more than by 2 %.

In the theory of SIT at the nondegenerate quantum transition, a bell-shaped input pulse is transformed in the medium into $n$ $2\pi$-pulses if the 'area' $\Theta_1$ under its real envelope lies in the interval between $(2n-1)\pi$ and $(2n+1)\pi$ [2]. In the case of SIT at the degenerate $J = 0 \leftrightarrow J = 1$ transition, this condition is valid when the area of a bell-shaped input elliptically polarised pulse is defined by the expression

$$\Theta_1 = \int_{-\infty}^{+\infty} a_1\sqrt{1 + \gamma_1^2}\,dw. \quad (9)$$

For linearly and circularly polarised radiations, expression (9) in the case of the bell-shaped envelope $a_1$ coincides with the pulse area in terms of the theory of SIT at nondegenerate quantum transitions.

## 3. Results of calculations

**3.1.** Let us set $\alpha_{10} = 0.5$, $\gamma_{10} = 0.3$, $a_{10} = 1.4367$, $\alpha_{20} = \pi/2$, and $\gamma_{20} = 0.3$ in (6) and (7). In the given case, both input radiations have the right-hand elliptic polarisation and the angle between the major axes of their PEs is approximately 60°. In this case, $\Theta_1 = 1.5\pi$, so that in the absence of signal radiation, the formation of a single $2\pi$ pulse in the pump channel is expected.

Figure 2 presents the dependences $W_l(s)$ and $I_l(s)$. The plateau in curves $W_1$ and $I_1$ for small $s$ is explained by the formation of the $2\pi$-pulse in the pump channel. The plateau in curves $W_2$ and $I_2$ for large $s$ corresponds to the free propagation of the signal pulse after the complete depletion of the pump energy. In this case, $I_2 < 0$, which means that signal radiation has predominantly left-hand elliptic polarisation.

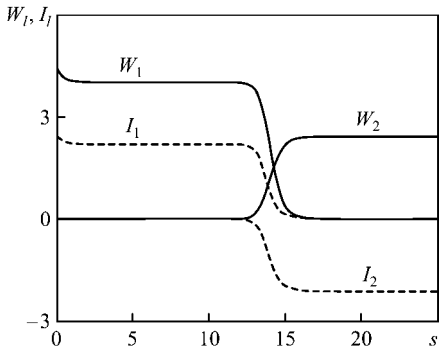


**Figure 2.** Energy (solid curves) and the $z$ component of the angular momentum (dashed curves) for the pump ($W_1$, $I_1$) and signal ($W_2$, $I_2$) pulses, respectively, as functions of the normalised coordinate $s$.

The evolution of the envelope of pump radiation is shown in Fig. 3. It follows from analysis using expression (8) that Figs 3b, c show the $2\pi$-pulse with a weak precursor pulse. The dependence in Fig. 3d was obtained for $s = 20$, when the pump energy is almost exhausted. The values of $\alpha_1$ and $\gamma_1$ remain invariable up to the distance at which the $2\pi$-pulse collapses ($s = 15$). However, the second pulse appearing at large distances due to the decay of the pump pulse (the right pulse in Fig. 3d) has the PE parameters that

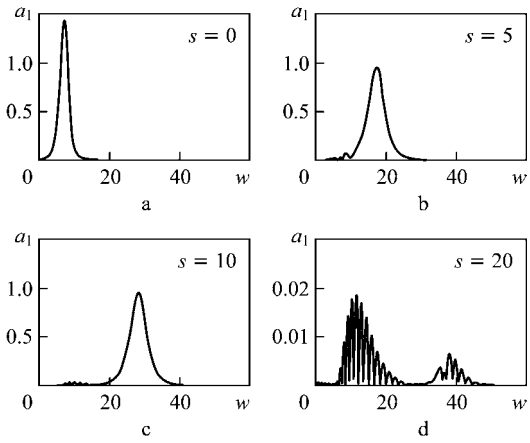


**Figure 3.** Evolution of the pump pulse envelope for different values of $s$.

depend on $s$ and $w$ in a complicated way. Because this pulse is weak, we will not describe in detail these dependences.

Figure 4 shows the evolution of the envelopes $a_2$ of angles $\alpha_2$ and the compression parameters $\gamma_2$ of signal radiation for several values of $s$. By treating the pulse front as its envelope front, note that the leading edge of the signal pulse at large distances (Figs. 4b, c, d) has the left-hand elliptic polarisation, close to the circular polarisation ($\gamma_2 \approx -0.7$). At the trailing edge, the PE first is flattened, then degenerates into a line ($\gamma_2 = 0$), and again becomes an ellipse, already with the right-hand polarisation ($\gamma_2 > 0$). In a greater part of the region, where the function $a_2$ noticeably differs from zero, the value of $\gamma_2$ is negative. Therefore, radiation with the left-hand circular polarisation dominates, in accordance with the results presented in Fig. 2. Thus, the direction of rotation of the electric field strength vector of signal radiation in the medium is opposite to that for the input pump radiation (these directions coincided at the input to the medium). In the region of the signal pulse, the calculation gives the value

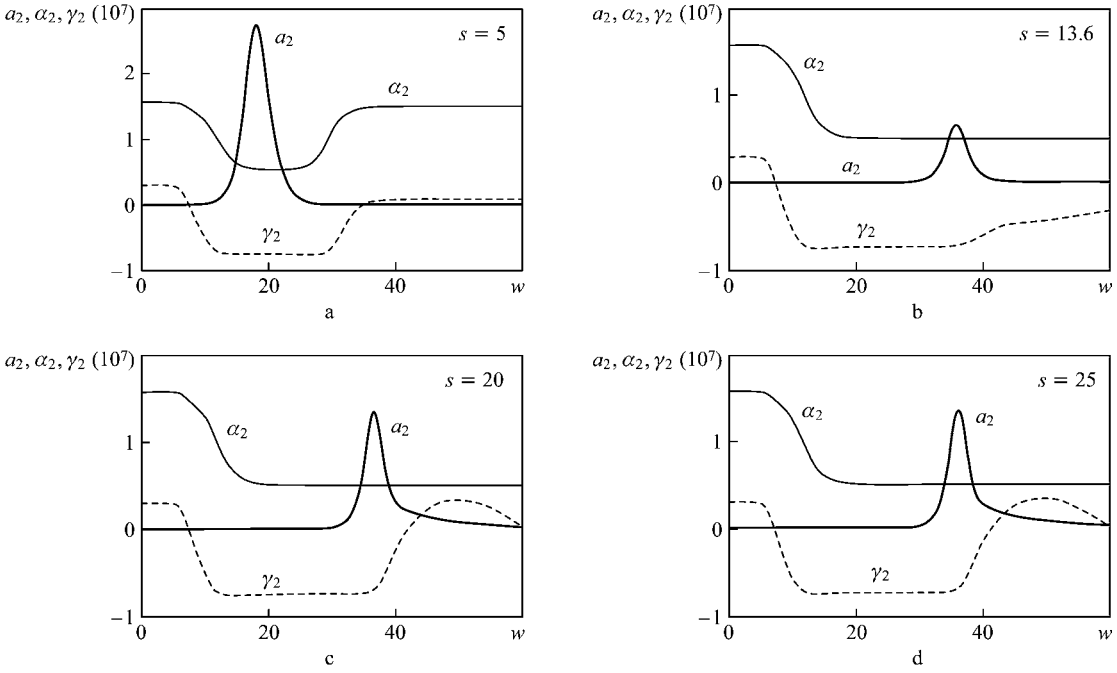


**Figure 4.** Evolution of the PE parameters for the signal pulse for different values of $s$.

$\alpha_2 = 0.5$. This means that the major axis of the signal radiation PE in the medium is parallel to that for the input pump radiation PE.

The appearance of the signal pulse with the left-hand polarisation is explained as follows. The input pump pulse has the right-hand elliptic polarisation ($\gamma_{10} = 0.3$). Therefore, right-hand-polarised radiation dominates in its decomposition into circularly polarised components. The right- and left-hand components, according to the known selection rules over the quantum number $M$, interact with the $1-2$ and $1-4$ transitions and are shown in Fig. 5 by long arrows tilted to the right and left, respectively. The more intense right-hand component is shown by the heavy arrow. Taking into account that the moduli of $p_{12}$ and $p_{14}$ of the electric dipole moments of the $1-2$ and $1-4$ transitions coincide, we can conclude that the $1-2$ transition plays the main role in the amplification of signal radiation.

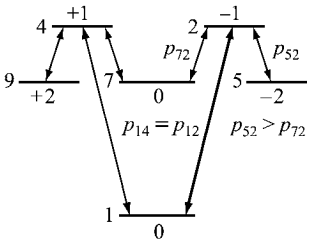


**Figure 5.** Scheme of quantum transitions. The numbers to the left of horizontal straight lines indicate the states according to Fig. 1, the numbers at the top (or bottom) are the quantum numbers of the corresponding states, $p_{ik}$ is the modulus of the electric dipole $i-k$ transition moment.

Signal radiation can be also presented as a sum of right- and left-hand circularly polarised components. The transitions related to these components are indicated in Fig. 5 by the short arrows tilted to the right and left, respectively. Due to the predominant excitation of state 2 (the heavy arrow in Fig. 5), the $5-2$ and $7-2$ transitions make the greatest contribution to the amplification of the signal pulse, the first transition providing the growth of the left-hand circularly polarised of the signal field, while the second transition providing the growth of the right-hand circularly polarised component. The moduli $p_{52}$ and $p_{72}$ of the electric dipole moments of these transitions are related by the expres-sion $p_{52} = \sqrt{6}\,p_{72}$ [25]. For this reason, the left-hand-polarised component of the signal field interacting with the $5-2$ transition is amplified stronger. As a result, signal radiation acquires the left-hand circular polarisation irrespective of the polarisation of the input signal pulse. Similarly, it can be readily shown that pump radiation with the left-hand elliptic polarisation will produce in the medium the signal pulse with the right-hand polarisation.

**3.2.** To elucidate the features of the evolution of $\alpha_2$ and $\gamma_2$ with changing $\gamma_{10}$, we performed a series of calculations which differed from previous calculations only by the values of $\gamma_{10}$. The results of the two of them, namely, for $\gamma_{10} = 0$ (linearly polarised pump pulse) and $\gamma_{10} = 0.8$ are presented in Figs 6a, b, respectively, for $s = 25$. A comparison of the dashed curves in these figures and Fig. 4d shows that the polarisation of the signal pulse approaches the left-hand circular polarisation with increasing $|\gamma_{10}|$. (For $\gamma_{10} = 0$, according to Fig. 6a, the signal is linearly polarised). The form of the

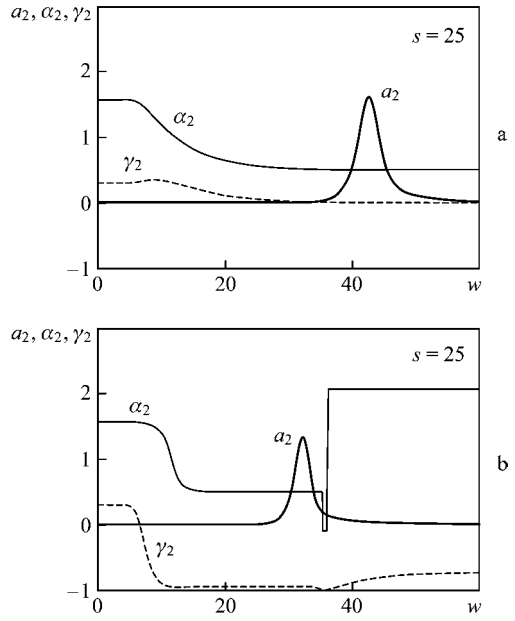


**Figure 6.** Evolution of the PE parameters of the signal pulse ($s = 25$) for $\gamma_{10} = 0$ (a) and $\gamma_{10} = 0.8$ (b).

dependences $\alpha_2(w)$ ($\alpha_2 = 0.5$ in the region where the pulse is located) suggests generally that the major axes of the signal and pump PEs are collinear. However, at the trailing edge of the pulse in Fig. 6b at the moment when polarisation becomes circular ($\gamma_2 = -1$, $\alpha_2 = -0.2$), the direction of the major axis of the PE changes jump-wise by the angle $\pi/2$ (the jump of the function after which $\alpha_2 = 2.071$).

**3.3.** Now we set $a_{10} = 3.8313$ in (7), retaining all the other conditions the same as in the calculation performed in paragraph 3.1. In this case $\Theta_1 = 4\pi$, so that, according to the discussion of (9), the formation of two $2\pi$-pulses is expected in the medium in the absence of signal radiation. Figure 7 presents the dependences of energies $W_1(s)$ and $W_2(s)$. The plateau in curve $W_1$ for small $s$ corresponds to the propagation of two $2\pi$-pulses in the pump channel in the virtual absence of signal radiation. The next plateau in curve $W_1$ and the plateau in curve $W_2$ located under the former plateau appear after the complete decay of the weaker pulse of the two $2\pi$-pulses and formation of a single signal radiation pulse. The last plateau in curve $W_2$ corresponds to the free

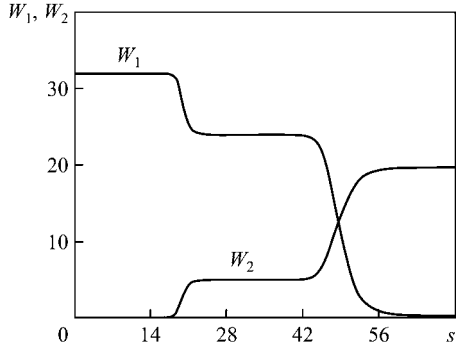


**Figure 7.** Pump pulse ($W_1$) and signal pulse ($W_2$) energies in the case of formation of two $2\pi$-pulses in the pump channel as functions of the normalised coordinate $s$.

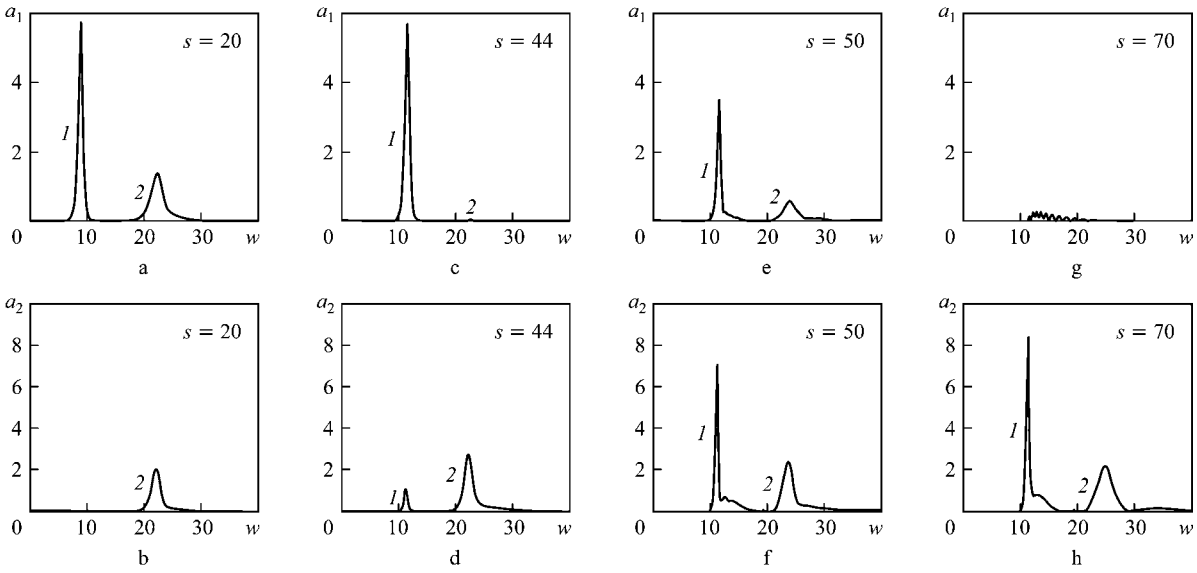


**Figure 8.** Evolution of the pump (a, c, e, g) and signal (b, d, f, h) pulse envelopes in the case of a high-power input pump pulse for different $s$.

propagation of two signal pulses after the depletion of pump radiation.

This is illustrated in Fig. 8 demonstrating the evolution of the envelopes $a_1$ and $a_2$ after the formation of two pump $2\pi$-pulses. Pulses (*1*) and (*2*) in Fig. 8a are the $2\pi$-pulses, the last of them being already in the decay stage. Signal pulse (*2*) produced by this $2\pi$-pulse is shown in Fig. 8b (the signal pulse produced by the first $2\pi$-pulse is unnoticeable at the scale in Fig. 8b). The results presented in Fig. 8c correspond to the distance at which the first pulse begins to decay, producing its own signal pulse [pulse (*1*) in Fig. 8d]. The number (*2*) in Fig. 8c indicates the region of extremely weak radiation remaining after the decay of the second $2\pi$-pulse. Signal pulse (*2*) produced from this pulse is shown in Fig. 8d.

Because pulse (*1*) in Fig. 8c noticeably differs from the $2\pi$-pulse, it leaves after itself the pump transition in the inverted state. By taking energy from this inversion, pulse (*2*) in Fig. 8c begins to be amplified, and as a result, the pump radiation again acquires the two-pulse structure (Fig. 8e). This process is accompanied by the growth of signal pulse (*1*) and some decrease in signal pulse (*2*) (cf. Figs 8e, f). At even larger distances, both pump pulses disappear (Fig. 8g), and two pulses of invariable shape remain at the signal frequency, which propagate at the speed of light in vacuum (Fig. 8h).

Figure 9a presents the temporal structure of pump radiation for $s = 50$. The pulse with the large peak amplitude of the envelope $a_1$ is the remnant of the decaying first pump $2\pi$-pulse. Its leading edge has the right-hand elliptic polarisation with the same values $\alpha_1$ and $\gamma_1$ ($\gamma_1 > 0$) as for the input pump pulse. At the trailing edge, as is shown by the curve for $\gamma_1$, the PE degenerates into a straight line ($\gamma_1 = 0$), and then polarisation becomes the left-hand elliptic ($\gamma_1 < 0$). At some instants, polarisation becomes the left-hand circular ($\gamma_1 = -1$), and in this case the major axis of the PE rotates jump-wise through the angle $\pi/2$ (the jump of function $\alpha_1$). The duration of the state with circular polarisation is so small that some regions in which $\alpha_1 = -0.2$ are unnoticeable at the scale of Fig. 9a.

The pulse with the smaller maximum value of the envelope $a_1$ appeared, as mentioned above, due to the amplification of the remnant of the second $2\pi$-pulse because of the population inversion at the pump transition. Its leading edge has the right-hand elliptic polarisation, which is even greater than that of the input pump pulse ($\gamma_1 > \gamma_{10}$). At the trailing edge, polarisation becomes the left-hand elliptic and sometimes the left-hand circular. As in the case of the first pulse, the major axis of the PE rotates jump-wise through the angle $\pi/2$.

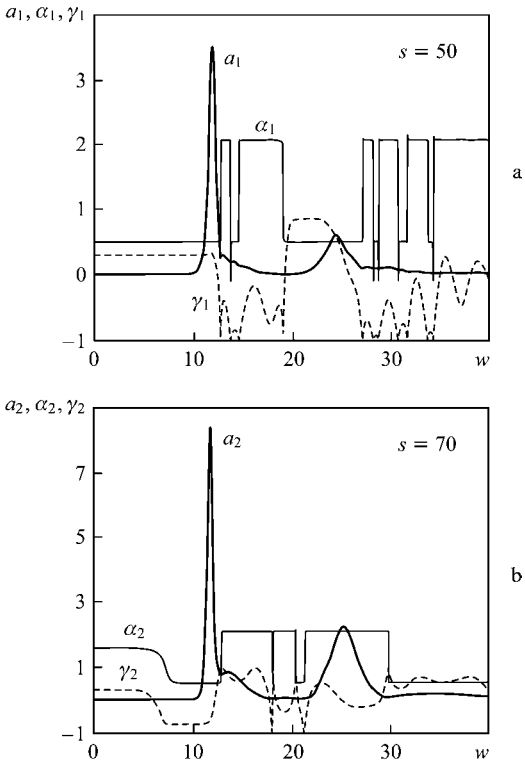


**Figure 9.** Structure of the pump (a) and signal (b) pulses.

Figure 9b presents the structure of signal radiation for $s = 70$. At the leading edge of the pulse with the large maximum amplitude of the envelope $a_2$, polarisation is the left-hand elliptic ($\gamma_2 < 0$), close to circular, the direction of the major axis of the PE being coincident with that for the input pump pulse ($\alpha_2 = \alpha_{10} = 0.5$). At the trailing edge, polarisation becomes the right-hand elliptic ($\gamma_2 > 0$). The pulse with the smaller maximum value of the envelope $a_2$ is characterised by a rather complicated change in the parameter $\gamma_2$, the major axis of its PE being perpendicular to that of the input pump pulse during almost the entire pulse duration ($\alpha_2 = 2.071$).

**3.4.** Let us set $\alpha_{10} = -0.2$, $\gamma_{10} = 1$, and $a_{10} = 1.0607$ in (6) and (7). In this case, the input pump pulse has the right-hand circular polarisation and has the same area $\Theta_1$ as the pump pulse in paragraph 3.1. As the boundary conditions for the signal, we set $\alpha_{20} = -0.2$, $a_{20} = 0.7071 \times 10^{-10}$ and one of the alternative conditions: $\gamma_{20} = -1$ or $+1$. In the first case, the input signal has the left-hand circular polarisation, while in the second case, it has the right-hand circular polarisation. The energy flux density of the input signal field is the same as in the calculation in paragraph 3.1.

Figure 10 presents the envelopes of the signal pulse at large distances $s$ for two indicated values of $\gamma_{20}$. A comparison of Figs 10a and 4c shows that the signal amplifications for $\gamma_{20} = -1$ and in calculations in paragraph 3.1 are approximately equal. However, for the same directions of the circular polarisation ($\gamma_{10} = \gamma_{20} = 1$) of input radiations, as follows from Fig. 10b, the amplification of the signal pulse in the medium is virtually absent, the maximum value of the signal envelope being more than $10^8$ times smaller than that in Fig. 10a.

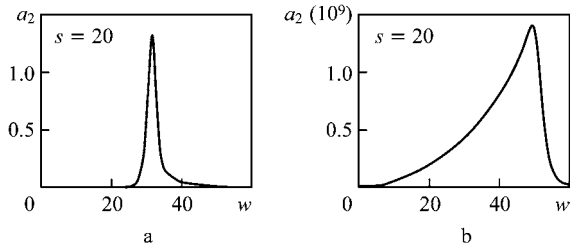


**Figure 10.** Signal pulse envelopes ($s = 20$) for $\gamma_{20} = -1$ (a) and 1 (b).

The physical nature of differences in the signal amplification for the opposite and the same directions of the circular polarisation of input radiations is demonstrated in Fig. 5, if we exclude the three arrows related to level 4. Then, the heavy arrow corresponds to the transition excited by pump radiation with the right-hand circular polarisation, which is the same in both cases. The thin arrow tilted to the left corresponds to the $5-2$ transition involved in the amplification of signal radiation in calculations with $\gamma_{20} = -1$ (the left-hand circular polarisation). The thin arrow tilted to the right corresponds to the $7-2$ transition responsible for the signal amplification in calculations with $\gamma_{20} = 1$ (the right-hand circular polarisation). As mentioned above, $p_{52}$ exceeds $p_{72}$ by a factor of $\sqrt{6}$.

Because the polarisation response of the medium is nonstationary, the pump pulse energy is transferred to the signal pulse at the trailing edge of the pump pulse. The pump pulse velocity is small compared to the speed of light in vacuum, and therefore the part of energy, which is transferred to the signal, shifts to the leading edge of the pump pulse, and the signal pulse duration tends to increase. The high rate of energy transfer to the trailing edge of the pulse for $\gamma_{20} = -1$, provided by the large value of $p_{52}$, causes the stabilisation of the pulse duration and the efficient amplification of the pulse. For $\gamma_{20} = 1$, due to the smallness of $p_{72}$, the rate of energy transfer to the trailing edge of the signal pulse is insufficient for such stabilisation. Therefore, the pulse duration continuously increases (see Fig. 10b) and a great part of energy 'leaves' the pump pulse region. This in turn leads to a considerable decrease in the signal growth rate.

**3.5.** Calculations, which we omit here, show that the signal pulse structure inside the medium at a large enough distance is independent of the structure of the input signal radiation, being determined only by the structure of the input pump pulse. This can be expected because the input signal radiation is assumed extremely weak. This circumstance suggests that the structures of signal pulses described in our calculations can be also realised when spontaneous emission plays the role of the input signal, i.e. in the case of resonance SRS in the filed of short laser pulses.

The results of our calculations also suggest that the qualitative features of the quasi-elliptic polarisation of signal radiation at a large enough distance from the input to the medium are independent of the profile of the bell-shaped pump pulse, being determined only by the interval $[(2n-1)\pi, (2n+1)\pi$, where $n = 0, 1, 2, \ldots]$ to which the area $\Theta_1$ of the input pump pulse falls.

Note finally that, if the right-hand polarisation of input pulses is replaced in calculations by the left-hand polarisation, and vice versa, the results remain invariable with accuracy to the same replacement of notations of polarisation states inside the medium.

**3.6.** Let us present some dimensional estimates. Consider the saturated vapours of the $^{208}$Pb isotope at temperature 950 K. In this case, $T_1 = 1.63 \times 10^{-10}$ s. By using the data on the relation between the saturated vapour pressure and the absolute temperature for lead [26], we obtain $N = 3.4 \times 10^{13}$ cm$^{-3}$, and using data [23] for the oscillator strengths of transitions in the $^{208}$Pb isotope, we find from the last expression in (3) that $z_0 = 0.03$ cm. The quantities $z_0$ and $T_1$ serve as normalisation parameters on passing from dimensional distances $z$ and time $t$ to dimensionless independent variables $s$ and $w$ by expressions (3). By using the relation $t = T_1 w$, which is valid, according to (3) for $z = 0$, we obtain that the input pump pulse duration (7) is approximately 0.4 ns, while the dimensionless distance $s = 70$ in Fig. 9b corresponds to the distance approximately 2 cm. Note that the value of $z_0$ strongly depends on the absolute temperature. Thus, $z_0 = 0.1$ cm at 900 K and 0.01 cm at 1000 K. On the contrary, the value of $T_1$ very weakly depends on temperature: $T_1 = 1.68 \times 10^{-10}$ s at 900 K and $1.59 \times 10^{-10}$ s at 1000 K.

The pump energy density (in kW cm$^{-2}$) can be estimated by the expression $P_1 = 1.3 a_1^2 (1 + \gamma_1^2)$. According to calculations in paragraphs 3.1 and 3.3, the peak intensity of the input pump pulse is 3 and 21 kW cm$^{-2}$, respectively.

As pointed out above, the condition $a_2 = 10^{-10}$ for the input pump pulse [see (7)] is not essential from the viewpoint of the validity of conclusions presented here. In other words, the lower is the input signal pulse intensity compared to the maximum intensity of the input pump pulse, the higher is the accuracy of our results. The energy flux density (in kW cm$^{-2}$) corresponding to the pulsed structures of the signal pre-

sented in our figures can be estimated by the expression $P_2 = 0.26a_2^2(1+\gamma_2^2)$. For the pulse in Fig. 4d, the maximum energy flux density is close to 0.7 kW cm$^{-2}$, while for the first pulse in Fig. 9b this density is approximately 27 kW cm$^{-2}$.

## 4. Conclusions

The main results of our investigations are as follows. The polarisation of the signal pulse in the medium is generally quasi-elliptic, with a slow (at the spatiotemporal scale of light oscillations) dependence of the orientation and eccentricity of its PE on time and distance. The type of this polarisation is independent of the structure of input signal radiation, when its intensity low enough, but is determined by the polarisation and intensity of input pump radiation. If the input pump pulse can produce a single $2\pi$-pulse in the medium (in the absence of signal radiation), then the major axes of PEs of both radiations are collinear. However, the directions of rotation of the electric field strengths of these radiations are opposite. At higher-power input pump pulses, the polarisation structure of the signal pulse in the medium is considerable complicated. This is explained by the complication of the evolution of the pump pulse under the action of forming signal radiation pulses.

Additional calculations have shown that the results presented in the paper remain qualitatively invariable for input pump pulses of different shapes and durations under the condition that their spectral width differs no more than by $2-3$ times from the inhomogeneous width of the transition in resonance with pump radiation. An increase (decrease) in the spectral width of the input laser pulse within this limits leads to the increase (decrease) of distances at which these effects can be observed.

The next step in the study of the double resonance in the $\Lambda$-scheme of the type considered here can be the simulation of polarisation effects when the power of input signal pulses is so high that the formation of the $2\pi$-pulse in the pump channel proves to be impossible even near the input to a resonance medium. Here, EIT can affect the polarisation of both radiations.

The results presented in this paper are obtained in the case of the exact resonance in the pump and signal channels, i.e. when the carrier frequencies of input signal and pump radiations are equal to the central frequencies of the corresponding inhomogeneously broadened transitions. The removal of this limitation also extends considerably the scope of investigations of polarisation effects in the case of the double resonance at degenerate quantum transitions.

## References


1. Manykin E.A., Samartsev V.V. *Opticheskaya ekho-spektroskopiya* (Optical Echo Spectroscopy) (Moscow: Nauka, 1984).
2. McCall S.L., Hahn E.L. *Phys. Rev.*, **183**, 457 (1968).
3. Fleishhauer M., Imamoglu A., Marangos J.P. *Rev. Mod. Phys.*, **77**, 633 (2005).
4. Rhodes C.K., Szöke A., Javan A. *Phys. Rev. Lett.*, **21**, 1151 (1968).
5. Gibbs H.M., McCall S.L., Salamo G.J. *Phys. Rev. A*, **12**, 1032 (1975).
6. Gun Xu, King T.A. *Phys. Rev. A*, **30**, 354 (1984).
7. Maimistov A.I., Basharov A.M., Elyutin S.O., Sklyarov Yu.M. *Phys. Reports*, **191**, 1 (1990).
8. Zelenskii I.V., Mironov V.A. *Zh. Eksp. Teor. Fiz.*, **121**, 1068 (2002).
9. Slavcheva G., Arnold J.M., Wallace I., Ziolkowski R.W. *Phys. Rev. A*, **66**, 063418 (2002).
10. Goren C., Wilson-Gordon A.D., Rosenbluh M., Friedmann H. *Phys. Rev. A*, **70**, 043814 (2004).
11. Lipsich A., Barriero S., Akulshin A.M., Lezama A. *Phys. Rev. A*, **61**, 053803 (2000).
12. Basharov A.M., Maimistov A.I. *Zh. Eksp. Teor. Fiz.*, **94**, 61 (1988).
13. Basharov A.M., Maimistov A.I. *Opt. Spektrosk.*, **68**, 1112 (1988).
14. Kasapi A., Maneesh J., Yin G.Y., Harris S.E. *Phys. Rev. Lett.*, **74**, 2447 (1995).
15. Arkhipkin V.G., Timofeev I.V. *Pis'ma Zh. Eksp. Teor. Fiz.*, **76**, 74 (2002).
16. Tarak N.D., Agarwal G.S. *Phys. Rev. A*, **67**, 033813 (2003).
17. Hansen K.R., Mølmer K. *Phys. Rev. A*, **75**, 053802 (2007).
18. Lukin V.D. *Rev. Mod. Phys.*, **75**, 457 (2003).
19. Eberly J.H., Rahman A., Grobe R. *Laser Phys.*, **6**, 69 (1996).
20. Arkhipkin V.G., Timofeev I.V. *Dokl. Ross. Akad. Nauk*, **401**, 467 (2005).
21. Larionov N.V., Sokolov I.M. *Kvantovaya Elektron.*, **37**, 1130 (2007) [*Quantum Electron.*, **37**, 1130 (2007)].
22. Wang B., Li S., Ma J., Wang H., Peng K.C., Xiao M. *Phys. Rev. A*, **73**, 051801 (2006).
23. De Zafra R.L., Marshall A. *Phys. Rev.*, **170**, 28 (1968).
24. Born M., Wolf E. *Principles of Optics* (Oxford: Pergamon Press, 1969; Moscow: Nauka, 1973).
25. Sobel'man I.I. *Introduction to the Theory of Atomic Spectra* (New York: Pergamon Press, 1972; Moscow: Nauka, 1977).
26. Grigor'ev I.S., Meilikhov E.Z. (Eds) *Fizicheskie velichiny. Spravochnik* (Handbook of Physical Quantities) (Moscow: Energoatomizdat, 1991).